RSC Advances

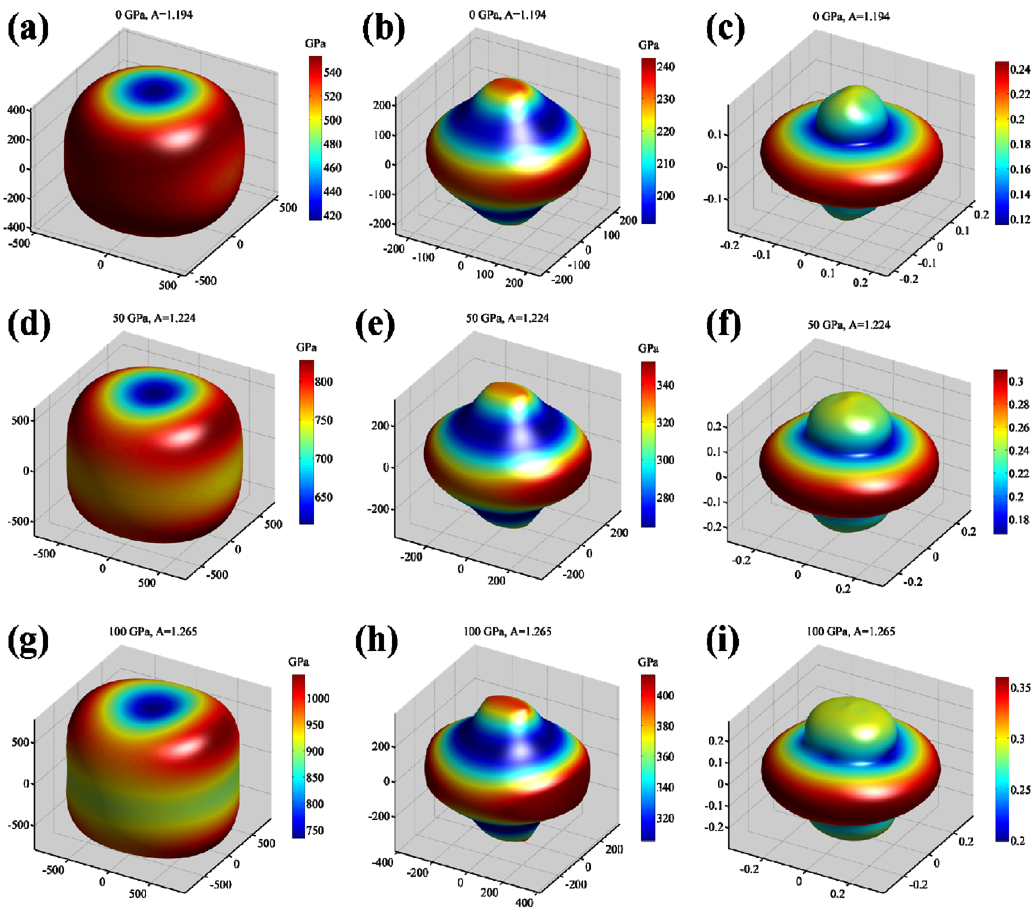
(a)
0 GPa, A=1.194
GPa
(b)
0 GPa, A=1.194
GPa
(c)
0 GPa, A=1.194
(d)
50 GPa, A=1.224
GPa
(e)
50 GPa, A=1.224
GPa
(f)
50 GPa, A=1.224
(g)
100 GPa, A=1.265
GPa
(h)
100 GPa, A=1.265
GPa
(i)
100 GPa, A=1.265

Anisotropy in elasticity and thermodynamic properties of zirconium tetraboride under high pressure

Ruru Hao,[a] Xinyu Zhang,[a*] Jiaqian Qin,[b*] Jinliang Ning, [a] Suhong Zhang,[a] Zhi Niu,[c] Mingzhen Ma,[a] Riping Liu[a]

[a]*State Key Laboratory of Metastable Materials Science and Technology, Yanshan University, Qinhuangdao 066004, P.R. China*

[b]*Metallurgy and Materials Science Research Institute, Chulalongkorn University, Bangkok 10330, Thailand*

[c]*College of mechanical engineering, Yanshan University, Qinhuangdao 066004, P.R. China*

Abstract

The recently predicted ZrB_4 with *Amm*2 orthorhombic structure has great scientific and technical significance owing to its novel B-Zr-B "sandwiches" layers bonding and evaluated high hardness. To better understand the performance of *Amm*2-ZrB_4, its elastic and thermodynamic properties under pressure and temperature are studied here by taking advantage of the first principles calculations in combination with the quasi-harmonic Debye model. It is found that ZrB_4 keeps brittleness and mechanical stability up to 100 GPa, possessing pronounced elastic anisotropy demonstrated by the elastic anisotropy factors, the direction-dependent Young's modulus, shear modulus and Poisson's ratio. The pressure and temperature dependences of the thermodynamics parameters including normalized volume V/V_0, bulk modulus, specific heat, Debye temperature, thermal expansion coefficient and Grüneisen parameter in wide temperature (0 ~ 1000 K) and pressures (0 ~ 50 GPa) ranges are obtained and discussed detailedly.

* Corresponding author: e-mail: xyzhang@ysu.edu.cn and jiaqianqin@gmail.com

Ⅰ. INTRODUCTION

In recent decades, transition metal borides (TMBs) have drawn considerable attention as candidate (super)hard materials, and a number of them have been widely used in high-temperature environments, cutting tools, and hard coating owing to their superior properties such as high strength, high hardness, ultra-incompressibility and good thermal stability.[1-4] Recently, novel transition metal (e.g., Fe,[5-7] W[8-10], and Cr,[3]) borides have been successfully synthesized under ambient or high pressure (65 GPa for Pnnm-FeB_4, 46.2 GPa for P63/mmc-WB_4 and 48 GPa for Pnnm-CrB_4) and extensive experimental and theoretical investigations have been carried out on these borides, which identifies their superhardness and leads to the low-cost synthesis of superhard materials. For the Zr-B system, there are three identified phases (ZrB, ZrB_2, and ZrB_{12}) according to the phase diagram.[11] The relatively high hardness of ZrB_2 and ZrB_{12} naturally leads us to wonder if there are any (super)hard zirconium tetraborides. Inspired by such a hypothesis, our group successfully predicted two new orthorhombic phases of ZrB_4 and estimated their hardness as 42.8 GPa and 42.6 GPa for *Cmcm* and *Amm*2 structure, respectively.[12] Both phases exhibit an interesting B–Zr–B sandwiches stacking order along the c and a-axis, and the sandwiches are connected by strong covalent bond (B-B bond). The three-dimensional networks of high atomic density consequently explained the occurrence of superhardness in ZrB_4. The two structures are similar, but we find that *Amm*2-ZrB_4 might be more easily obtained due to its lower formation enthalpy. These facts stimulate us to conduct a detailed investigation on its fundamental properties, such as elastic constants, elastic anisotropy and thermodynamic properties which are crucial to its practical applications and synthesis. For example, the elastic constants of a solid give important information concerning the nature of the forces operating in the solid[13, 14] and help us to understand its mechanical behaviors in practical application, such as anisotropy, phase transformation, elastic instability, plastic deformation and fracture, precipitation, dislocation dynamics, crack and so on[15]. On the other hand, the understanding of thermodynamic properties of solids (such as heat capacity, thermal expansion coefficient, Grüneisen parameters, and Debye temperature) will be beneficial to their synthesis and practical applications[16]. Therefore, in this paper, elastic properties of ZrB_4 coupled with thermodynamic properties at various temperatures and pressures are investigated systematically through the first principles calculations and quasi-harmonic Debye model[17].

This paper proceeds as follows: the details of the calculation methods and theoretical model are described in Sec. II, followed by the calculated results and analysis in Sec. III. Conclusions are summarized in Sec. IV.

Ⅱ. METHODS OF CALCULATION

The *ab initio* calculations were performed using density functional theory within the generalized gradient approximation (GGA),[18] as implemented in the Vienna *ab initio* simulation package (VASP)[19]. The exchange and correlation potential was treated by the generalized gradient approximation in the scheme of Perdew-Burke-Ernzerhof (PBE).[20] The all-electron projector augmented wave (PAW) method[21] was employed with a plane-wave cutoff energy of 600 eV. The k-point grid in the Brillouin zone were generated using the Monkhorst-Pack scheme with the separation of 0.03 Å^{-1}. The total energy convergence tests showed that convergence to within 1 meV/atom was achieved with the above calculation parameters. Single crystal elastic constants were calculated via a strain-stress approach. i.e., by applying a small strain to the equilibrium lattice of orthorhombic unit cell and fitting the dependence of the resulting change in stress on the strain. The bulk modulus, shear modulus, Young's modulus, and Poisson's ratio were determined by using the Voigt-Reuss-Hill approximation[22], in which the Voigt and Reuss expressions represent the upper and lower limit of the polycrystalline modulus. The formulae for orthorhombic structure are:

$$B_V = [c_{11} + c_{22} + c_{33} + 2(c_{12} + c_{13} + c_{23})]/9,$$

$$G_V = [c_{11} + c_{22} + c_{33} + 3(c_{44} + c_{55} + c_{66}) - (c_{12} + c_{13} + c_{23})]/15,$$

$$\begin{aligned} B_R = \Delta/[&c_{11}(c_{22} + c_{33} - 2c_{23}) + c_{22}(c_{33} - 2c_{13}) - 2c_{33}c_{12} + c_{12}(2c_{23} - c_{12}) \\ &+ c_{13}(2c_{12} - c_{13}) + c_{23}(2c_{13} - c_{23})] \end{aligned},$$

$$\begin{aligned} G_R = 15/\{4[&c_{11}(c_{22} + c_{33} + c_{23}) + c_{22}(c_{33} + c_{13}) + c_{33}c_{12} - c_{12}(c_{23} + c_{12}) \\ &- c_{13}(c_{12} + c_{13}) - c_{23}(c_{13} + c_{23})]/\Delta + 3(1/c_{44} + 1/c_{55} + 1/c_{66})\} \end{aligned},$$

$$\Delta = c_{13}(c_{12}c_{23} - c_{13}c_{22}) + c_{23}(c_{12}c_{13} - c_{23}c_{11}) + c_{33}(c_{11}c_{22} - 2c_{12}{}^2),$$

$$B = (B_R + B_V)/2, \quad G = (G_R + G_V)/2. \qquad (1)$$

The Young's modulus E and the Poisson's ratio υ are then calculated from the elastic moduli using the following relations:

$$E = \frac{9BG}{3B + G}, \quad \nu = \frac{3B - 2G}{2(3B + G)} \qquad (2)$$

Ⅲ. RESULTS AND DISCUSSION

3.1 Elastic properties

The lately predicted crystal structure of ZrB_4 is orthorhombic with space group *Amm*2, No. 38, with 20 atoms per conventional unit cell consisting of four ZrB_4 f.u. in a unit cell, in which one Zr and three B atoms occupy the Wyckoff position 8*f* (0.3461, 0.6689, 0.2655), 4*c* (0.8289, 0.5, 0.7469), 4*e* (0.5, 0.3374, 0.9792), and 4*d* (0, 0.3332, 0.2486) respectively. The equilibrium lattice constants, volume per formula unit, density, bulk modulus and its pressure derivative are all listed in Table 1, together with available experimental and theoretical results of ZrB_2 and ZrB_{12} for comparison. In the elastic range, due to the symmetry of the crystal, there are nine independent components in the elastic tensor for ZrB_4, i.e., C_{11}, C_{22}, C_{33}, C_{44}, C_{55}, C_{66}, C_{12}, C_{13} and C_{23}. Elastic constants play important roles in providing a deeper insight into mechanical stability and stiffness of materials[23]. The pressure dependences of the elastic constants up to 100 GPa are illustrated in Fig. 1. It can be seen that all elastic constants increase monotonically with pressure and all C_{ij} satisfy the well-known Born stability criteria[24] up to 100 GPa, which indicates that ZrB_4 is still mechanically stable at high pressure of 100 GPa.

$$C_{11}>0,\ C_{22}>0,\ C_{33}>0,\ C_{44}>0,\ C_{55}>0,\ C_{66}>0,$$
$$(C_{11}+C_{22}-2C_{12})>0,(C_{11}+C_{33}-2C_{13})>0,(C_{22}+C_{33}-2C_{23})>0,$$
$$C_{11}+C_{22}+C_{33}+2C_{12}+2C_{13}+2C_{23}>0. \tag{3}$$

Unfortunately, there are no experimental data available for comparison present, therefore, our results could be a reference for future studies and applications under high pressures of ZrB_4.

In general, the large value of shear modulus is an indication of more pronounced directional bonding between atoms, and the Poisson's ratio is a factor that measures the stability of a crystal against shear and Young's modulus provides a measure of stiffness of a solid. The calculated elastic constants, elastic moduli (*B*, *G* and *E*), Poisson's ratio υ and the *B*/*G* ratio of ZrB_4 under pressure are given in Table 2, along with the theoretical values of other transition metal tetraborides (WB_4, CrB_4, FeB_4). It is shown in Table 2 that all of the *B*, *G*, *E*, υ and *B/G* increase substantially with pressure and the calculated bulk and shear moduli of *Amm*2-ZrB_4 are comparable to those of WB_4, CrB_4, FeB_4, indicating their strong ability to resist volume deformation. According to Pugh's criterion,[25] a low (high) *B*/*G* value is associated with brittleness (ductility), and the ductile and brittle materials are separated by the critical value (1.75). The *B*/*G* of ZrB_4 reaches 1.47 at 100 GPa, implying that ZrB_4 is a brittle and mechanically stable phase within the range of pressures.

Debye temperature θ_D is a fundamental parameter of a compound, which has close relationships with specific heat, melting temperature, and elastic constants. The θ_D can be calculated from elastic constants ($\theta_D = \frac{h}{k}\left[\frac{3n}{4\pi}\left(\frac{\rho N_A}{M}\right)\right]^{\frac{1}{3}} v_m$),[33] which gives explicit information about the lattice vibrations.[34] The Debye temperature of ZrB_4 under pressure is presented in Table 3, showing an increasing trend with pressure. As is generally known, a crystal with a larger Debye temperature corresponds to a stiffer characteristic. This is because the optical phonons have a higher frequency and therefore require greater energy to activate. Pressure typically enhances the interactions between atoms of a crystal and hence stiffers it, which is manifested by increased elastic moduli *B* and *G*. Therefore, pressure typically increases Debye temperature of ZrB_4 and this implies stronger interactions between atoms in the system.

3.2 Elastic anisotropy

Elastic anisotropy is very important in diverse applications of materials, such as phase transformations, precipitation, dislocation dynamics and microcrack formation. The fundamental information about the bonding characteristics between adjacent atomic planes can also be obtained via the elastic anisotropy. Therefore, this property will be crucial for the potential hard material ZrB_4. The shear anisotropy factors (A_1, A_2, A_3), the universal elastic anisotropy index A^U and the directional bulk modulus B_a, B_b and B_c are appropriate measures to quantify the extent of anisotropy.[35] The shear anisotropy factor for the $\{100\}$ shear planes between the <011> and <010> directions is defined as

$$A_1 = \frac{4C_{44}}{C_{11} + C_{33} - 2C_{13}}, \tag{4}$$

for the $\{010\}$ shear planes between the <101> and <001> directions is

$$A_2 = \frac{4C_{55}}{C_{22} + C_{33} - 2C_{23}}, \tag{5}$$

for the $\{001\}$ shear planes between the <110> and <010> directions is

$$A_3 = \frac{4C_{66}}{C_{11} + C_{22} - 2C_{12}}, \tag{6}$$

for the universal elastic anisotropy index A^U, defined by Ranganathan and Ostoja-Starzewski from the bulk modulus B and shear modulus G denoted by Voigt and Reuss approaches,[35] is

$$A^U = 5\frac{G_V}{G_R} + \frac{B_V}{B_R} - 6, \qquad (7)$$

and the directional bulk modulus along different crystallographic axis can be defined as[36]

$$B_i = i\left(dP/di\right) \;\; (i = a, b, \text{ and } c) \qquad (8)$$

Taking advantage of the formulae mentioned above, the parameters about elastic anisotropy (A_1, A_2, A_3, A^U, B_a, B_b and B_c) are calculated and presented in Table 4. In the case of isotropic crystals, A_1, A_2, and A_3 are all equal to 1, while any deviation from one means the amplitude of anisotropy of the crystal. From Table 4, we can see that A_1, A_2, and A_3 are larger than 1 at 0 GPa and all increase with pressure. The shear anisotropy results of ZrB_4 indicate that the elastic anisotropy for the $\{010\}$ shear planes between the <101> and <001> directions is more obvious than that of the $\{100\}$ shear planes between the <011> and <010> directions and the $\{001\}$ shear planes between the <110> and <010> directions, and the value of A_3 also reveals that ZrB_4 is nearly isotropic in $\{001\}$ shear planes. Because *Amm*2-ZrB_4 is orthorhombic, the shear anisotropy factors are not adequate to sufficiently describe its elastic anisotropy. Therefore, the universal elastic anisotropy index A^U should also be considered (A^U is zero for isotropic crystals). In Table 4, A^U is 0.09 at 0 GPa, which increases with increasing pressure. Meanwhile, the directional bulk modulus (B_a, B_b, B_c) also increases with pressure and the bulk modulus along the *c*-axis is larger than that along *a*-axis and *b*-axis at 100 GPa.

Although the factors calculated above have already conveyed that the elastic properties of ZrB_4 are anisotropic, it is still necessary to characterize the mechanical anisotropy in a more straightforward way. The shape of the 3D curved surface is sphere for isotropic materials ($A^{U} = 0$), but for anisotropic materials, the sphere will deform. The degree of deformation reflects the extent of anisotropy, and the variation of elastic modulus with direction can be demonstrated. Therefore the Young's modulus, Shear modulus, and Poisson's ratio along different directions in three-dimensional (3D) space as well as the projections in (-110) plane and (001) plane at pressures 0 GPa, 50 GPa and 100 GPa have been drawn to denote the elastic anisotropy of ZrB_4 on crystallographic directions, as is shown in Fig. 2 and Fig. 3. The direction dependent Young's modulus (E), Shear modulus (G) and Poisson's ratio (υ) for orthorhombic crystals[36, 37] can be defined respectively as:

Young's modulus:

$$E^{-1} = s'_{11} = s_{11}l_1^{\,4} + s_{22}l_2^{\,4} + s_{33}l_3^{\,4} + 2s_{12}l_1^{\,2}l_2^{\,2} + 2s_{23}l_2^{\,2}l_3^{\,2} + 2s_{13}l_1^{\,2}l_3^{\,2} + s_{44}l_2^{\,2}l_3^{\,2} + s_{55}l_1^{\,2}l_3^{\,2} + s_{66}l_1^{\,2}l_2^{\,2} \tag{9}$$

Shear modulus:

$$\begin{aligned} G^{-1} &= 4s_{11}l_1^{\,2}m_1^{\,2} + 4s_{22}l_2^{\,2}m_2^{\,2} + 4s_{33}l_3^{\,2}m_3^{\,2} + 8s_{12}l_1m_1l_2m_2 + 8s_{23}l_2m_2l_3m_3 + 8s_{13}l_1m_1l_3m_3 + \\ &s_{44}(l_2m_3 + m_2l_3)^2 + s_{55}(l_1m_3 + m_1l_3)^2 + s_{66}(l_1m_2 + m_1l_2)^2 \end{aligned} \tag{10}$$

Poisson's ratio:

$$\begin{aligned} s'_{12} &= l_1^{\,2}m_1^{\,2}s_{11} + (l_1^{\,2}m_2^{\,2} + l_2^{\,2}m_1^{\,2})s_{12} + (l_1^{\,2}m_3^{\,2} + l_3^{\,2}m_1^{\,2})s_{13} + l_2^{\,2}m_2^{\,2}s_{22} + (l_2^{\,2}m_3^{\,2} + l_3^{\,2}m_2^{\,2})s_{23} \\ &+ l_3^{\,2}m_3^{\,2}s_{33} + l_2l_3m_2m_3s_{44} + l_1l_3m_1m_3s_{55} + l_1l_2m_1m_2s_{66} \end{aligned} \tag{11}$$

$$\upsilon = -\frac{s'_{12}}{s'_{11}} \tag{12}$$

where s_{ij} is the usual elastic compliance constants, l_i is the direction cosines in any arbitrary direction and m_i is the direction cosines in perpendicular direction. From Fig. 2, elastic anisotropy is clearly seen in ZrB_4, and the greater the pressure, the more obvious the anisotropy. In addition, the magnitude of Young's modulus in a specific direction can also be used to indicate the strength of chemical bonds in that direction. In Fig. 2(a), (d) and (g), the maximum of Young's modulus is observed in <111> direction, and the minimum occurs in <001> direction. Because a larger Young's modulus often stands for more covalent feature of a material,[38, 39] we can substantiate that the covalent feature of the bonding in <111> direction is more dominant than other directions. The *G* is remarkably dependent on the stress direction (Fig. 2(b), (e) and (h)) with the highest (lowest) value in the [001] ([111]) direction, and the Poisson's ratio (Fig. 2(c), (f) and (i)) has similar characteristics. Fig. 3(a) and (b) show the orientation dependence of *E* and *G* changing from [001] to [110] direction in (-110) plane and from [100] to [010] direction in (001) plane under different pressures, and the shape of the projections in (001) plane at 0 GPa, 50 GPa, 100 GPa is almost round, which illustrates that ZrB_4 is nearly isotropic in (001) plane. This result is consistent with the shear anisotropy factor A_3. Poisson's ratio represents the negative ratio of transverse and longitudinal strains which plays a significant role in mechanical engineering design.[40] The values of υ in (-110) plane varies in a very large range as shown in Fig. 3(c), the features of υ under 100 GPa are $0.283 < \upsilon < 0.381$ in (-110) plane. It means that when the stress direction is perpendicular to the (-110) plane, the maximum strain is noted in the [001] direction and the minimum strain in the [111] direction.

3.3 Thermodynamic properties

The thermodynamic properties of ZrB_4 at various temperatures (0 ~ 1000 K) and pressures (0 ~ 50 GPa) are systematically calculated. In Fig. 4, we present the normalized volume-pressure and bulk modulus-pressure diagram of ZrB_4 at temperatures 0, 200, 400, 600, 800, and 1000 K, where V_0 is the zero-pressure equilibrium volume. It is easily seen from Fig. 4 that, as pressure increases, the relative volume V/V_0 decreases at a given temperature and the V/V_0 curve becomes steeper with temperature increasing, which implies that ZrB_4 is more easily compressed when temperature increases. Furthermore, it is found that the bulk modulus increases with pressure at a constant temperature and decreases with temperature at a given pressure.

The calculated heat capacity of ZrB_4 as a function of temperature (pressure) at given pressure (temperature) is demonstrated in Fig. 5. It is shown in Fig. 5(a) that the heat capacity C_V fits T^3 term in their sufficiently low-temperature regions and approximates to absolute zero when the temperature vanishes at the given 0, 10, 20, 30, 40, 50 GPa. This is due to the harmonic approximations of the Debye model used here. At intermediate temperatures, the temperature dependence of C_V is dominated by the details of vibrations of atoms.[41] At high temperatures, the calculated C_V is expected to get close to the Dulong-Petit limit, $3nN_Ak_B$ (n is the number of atoms in a molecule, N_A is the Avogadro constant and k_B is the Boltzmann constant), which is common to all solids at high temperatures. For ZrB_4, the Dulong-Petit limit is about 120 J/mol*K. The pressure dependence of the heat capacity for ZrB_4 at 100, 200, 400, 600, 800 and 1000 K is presented in Fig. 5(b). It is noted that the calculated C_V decreases with pressure at a constant temperature and increases with temperature at a given pressure. From Fig. 5(a) and (b), we can get that the effect of temperature on C_V is greater than that of pressure.

The volume thermal expansion coefficient α as a function of temperature (pressure) at different pressures (temperatures) is shown in Fig. 6(a) and (b). Because of the weak dependence of the bulk modulus on temperature and that α is proportional to C_V ($\alpha = \frac{\gamma C_V}{3K}$, γ is the Gruneisen parameter, and K is the bulk modulus), the trend of the volume thermal expansion coefficient is similar to the heat capacity. As shown in Fig. 6(a), at given pressures, α increases rapidly with temperature at sufficiently low temperatures (α(T) ~ T^3) and gradually turns to a slow increase at high temperatures (T > 400 K). Additionally, it is noted in Fig. 6(b) that α decreases with increasing pressure at a constant temperature, and the trend slows down at high pressures.

Figure 7 shows the pressure dependence of the Debye temperature θ_D and Grüneisen parameter γ of ZrB_4 at different temperatures (0, 100, 200, 400, 600, 800, and 1000 K). It is easily seen in Fig. 7(a) that when temperature keeps constant, Debye temperature increases almost linearly with increasing pressure and compared with pressure, the variation of θ_D caused by temperature is very small. Therefore, we can draw a conclusion that the effect of the temperature on θ_D is not as significant as that of pressure. In quasi-harmonic Debye model, Grüneisen parameter γ describes the anharmonic effects of the crystal lattice thermal vibration. From Fig. 7(b), we can see that at fixed temperature, γ decreases sharply with pressure, and as temperature goes higher, γ decreases more rapidly with the increase of pressure.

□. CONCLUSION

In conclusion, we have focused our attention on prediction and detailed analysis of elastic constants, anisotropic properties, and thermodynamic properties under high pressures of *Amm*2-ZrB_4 by first principles calculations in combination with the quasi-harmonic Debye model in this work. In the light of the Born stability criteria and the Pugh criterion, ZrB_4 (*Amm*2) is mechanically stable and exhibits brittle nature within the scope of the studied pressure (0 ~ 100 GPa). The Debye temperature of ZrB_4 was calculated by taking advantage of the relationship that Θ is proportional to the averaged sound velocity v_m, and it increases with pressure. Young's modulus, shear modulus and Poisson's ratio as a function of crystal orientation have been systematically investigated and analyzed. ZrB_4 exhibits pronounced elastic anisotropy and the extent increases with pressure. Furthermore, the pressure and temperature dependences of calculated normalized volume V/V_0, bulk modulus, volume thermal expansion coefficient, specific heat, Debye temperature, and Grüneisen parameter have also been evaluated in the ranges of 0 ~ 50 GPa and 0 ~ 1000 K through quasi-harmonic Debye model. The results point out that pressure and temperature have manifest effects on these thermodynamic properties. The present study provides detailed and systematic information for *Amm*2-ZrB_4, which is of fundamental importance for its industrial application.

Acknowledgments

This work was supported by the NBRPC (grant 2013CB733000), NSFC (grants 51171160/51434008/11447243). S. Z would like to acknowledge support by the Natural Science Foundation of Hebei province (grant E2015203200).

References

1. Q. Gu, G. Krauss and W. Steurer, *Adv. Mater.*, 2008, **20**, 3620.
2. A. R. Oganov, J. Chen, C. Gatti, Y. Ma, Y. Ma, C. W. Glass, Z. Liu, T. Yu, O. O. Kurakevych and V. L. Solozhenko, *Nature*, 2009, **457**, 863.
3. H. Niu, J. Wang, X.-Q. Chen, D. Li, Y. Li, P. Lazar, R. Podloucky and A. N. Kolmogorov, *Phys. Rev. B*, 2012, **85**, 144116.
4. J. Haines, J. Leger and G. Bocquillon, *Ann. Rev. Mater. Res.*, 2001, **31**, 1.
5. X. Zhang, J. Qin, J. Ning, X. Sun, X. Li, M. Ma and R. Liu, *J. Appl. Phys.*, 2013, **114**, 183517.
6. X. Zhang, J. Qin, Y. Xue, S. Zhang, Q. Jing, M. Ma and R. Liu, *Phys. Status Solidi RRL*, 2013, **7**, 1022.
7. H. Gou, N. Dubrovinskaia, E. Bykova, A. A. Tsirlin, D. Kasinathan, W. Schnelle, A. Richter, M. Merlini, M. Hanfland and A. M. Abakumov, *Phys. Rev. Lett.*, 2013, **111**, 157002.
8. Y. Chen, D. He, J. Qin, Z. Kou, S. Wang and J. Wang, *J. Mater. Res.*, 2010, **25**, 637.
9. C. Liu, F. Peng, N. Tan, J. Liu, F. Li, J. Qin, J. Wang, Q. W. He and Duanwei, *High Pressure Res.*, 2011, **31**, 275.
10. M. Wang, Y. Li, T. Cui, Y. Ma and G. Zou, *Appl. Phys. Lett.*, 2008, **93**, 101905.
11. T. Tokunaga, K. Terashima, H. Ohtani and M. Hasebe, *Mater. Trans.*, 2008, **49**, 2534.
12. X. Zhang, J. Qin, X. Sun, Y. Xue, M. Ma and R. Liu, *Phys. Chem. Chem. Phys.*, 2013, **15**, 20894.

13. N. Korozlu, K. Colakoglu, E. Deligoz and S. Aydin, *J. Alloy. Compd.*, 2013, 157.

14. S. Zhang, X. Zhang, Y. Zhu, S. Zhang, L. Qi and R. Liu, *Intermetallics.*, 2014, **44**, 31.

15. X. Zhang, J. Qin, T. Perasinjaroen, W. Aeksen, M. K. Das, R. Hao, B. Zhang, P. Wangyao, Y. Boonyongmaneerat, S. Limpanart, M. Ma and R. Liu, *Surf. Coat. Tech.*, 2015, **276**, 228.

16. R. Hao, X. Zhang, J. Qin, S. Zhang, J. Ning, N. Sun, M. Ma and R. Liu, *RSC Advances*, 2015, **5**, 36779.

17. M. Blanco, E. Francisco and V. Luana, *Comput. Phys. Commun.*, 2004, **158**, 57.

18. J. P. Perdew, K. Burke and M. Ernzerhof, *Phys. Rev. Lett.*, 1996, **77**, 3865.

19. G. Kresse and J. Furthmüller, *Phys. Rev. B*, 1996, **54**, 11169.

20. J. P. Perdew, K. Burke and M. Ernzerhof, *Phys. Rev. Lett.*, 1996, **77**, 3865.

21. G. Kresse and D. Joubert, *Phys. Rev. B*, 1999, **59**, 1758.

22. R. Hill, *Proc. Phys. Soc. A*, 1952, **65**, 349.

23. S. Zhang, X. Zhang, Y. Zhu, M. Ma, J. Qin and R. Liu, *Mater. Chem. Phys.*, 2015, **149–150**, 553.

24. M. Born, *Proc. Camb. Phil. Soc*, 1940, **36**, 160.

25. S. F. Pugh, *Philos. Mag.*, 1954, **45**, 823.

26. P. Vinet, J. H. Rose, J. Ferrante and J. R. Smith, *J. Phys.: Condens. Matter*, 1989, **1**, 1941.

27. F. Birch, *Phys. Rev.*, 1947, **71**, 809.

28. F. D. Murnaghan, *Am. J. Math.*, 1937, 235.

29. H. Fu, M. Teng, X. Hong, Y. Lu and T. Gao, *Physica B: Condens. Matter*, 2010, **405**, 846.

30. A. Rybina, K. Nemkovski, P. Alekseev, J.-M. Mignot, E. Clementyev, M. Johnson, L. Capogna, A. Dukhnenko, A. Lyashenko and V. Filippov, *Phys. Rev. B*, 2010, **82**, 024302.

31. A. Pereira, C. Perottoni, J. da Jornada, J. Leger and J. Haines, *J. Phys.: Condens. Matter*, 2002, **14**, 10615.

32. N. L. Okamoto, M. Kusakari, K. Tanaka, H. Inui, M. Yamaguchi and S. Otani, *J. Appl. Phys.*, 2003, **93**, 88.

33. O. L. Anderson, *J. Phys. Chem. Solids*, 1963, **24**, 909.

34. J. Jia, D. Zhou, J. Zhang, F. Zhang, Z. Lu and C. Pu, *Comp. Mater. Sci.*, 2014, **95**, 228.

35. S. I. Ranganathan and M. Ostoja-Starzewski, *Phys. Rev. Lett.*, 2008, **101**, 055504.

36. P. Ravindran, L. Fast, P. Korzhavyi, B. Johansson, J. Wills and O. Eriksson, *J. Appl. Phys.*, 1998, **84**, 4891.

37. J. F. Nye, *Physical Properties of Crystals: Their Representation by Tensors and Matrices*, Oxford University Press, Oxford, 1985.

38. M. Rajagopalan, S. P. Kumar and R. Anuthama, *Physica B: Condens. Matter*, 2010, **405**, 1817.

39. G. Yi, X. Zhang, J. Qin, J. Ning, S. Zhang, M. Ma and R. Liu, *J. Alloy. Compd.*, 2015, **640**, 455.

40. J. Lewandowski, W. Wang and A. Greer, *Phil. Mag. Lett.*, 2005, **85**, 77.

41. Z. Huang, J. Feng and W. Pan, *Comp. Mater. Sci.*, 2011, **50**, 3056.

Table 1. The calculated equilibrium lattice constants a_0, b_0, c_0 (Å) and equilibrium volume per formula unit V_0 (Å^3), density ρ, EOS fitted bulk modulus B_0 (GPa), and its pressure derivative B_0' for the orthorhombic ZrB_4 at 0 K and 0 GPa.

		a_0	b_0	c_0	V_0	ρ	B_0	B_0'
ZrB_4	This work	10.3120	5.41307	3.17999	300	5.03	239[a], 238[b], 235[c]	3.84[a], 3.86[b], 3.90[c]
ZrB_2	Theo.	3.1768[d]	--	3.559[d]	31.1[d]	--	355[d]	4.2[d]
	Exp.	3.170[d]	--	3.532[d]	30.74[d]	--	317[f], 245[g]	--
ZrB_{12}	Theo.	7.415[e]	--	--	407.69[e]	--	--	--
	Exp.	7.4077[e]	--	--	406.49[e]	--	--	--

[a]Vinet universal EOS[26].
[b]Birch-Murnaghan 3rd-order EOS[27].
[c]Murnaghan EOS[28].
[d]Reference[29].
[e]Reference[30].
[f]Reference[31].
[g]Reference[32].

Table 2. The elastic constants C_{ij} (GPa), bulk modulus B (GPa), shear modulus G (GPa), Young's modulus E (GPa), Poisson's ratio υ, the B/G ratio and the H_v of ZrB_4 under pressure.

	P	C_{11}	C_{22}	C_{33}	C_{44}	C_{55}	C_{66}	C_{12}	C_{13}	C_{23}	B	G	E	v	B/G
ZrB_4	0	559	578	458	233	243	262	53	118	113	239	232	528	0.134	1.03
	10	618	625	517	256	270	283	75	146	139	275	253	581	0.149	1.09
	20	674	681	572	278	295	301	97	173	166	311	271	631	0.162	1.15
	30	740	750	638	297	318	324	108	194	190	346	294	687	0.169	1.18
	40	790	801	689	314	340	339	128	221	217	379	310	731	0.179	1.22
	50	838	849	736	330	361	353	148	249	245	412	324	770	0.188	1.27
	60	885	896	780	345	381	366	168	275	272	443	338	808	0.196	1.31
	70	929	940	829	359	401	378	188	302	300	475	351	845	0.204	1.35
	80	972	984	875	372	419	389.	207	329	327	506	363	879	0.211	1.40
	90	1016	1027	912	384	438	404	226	356	354	536	375	912.	0.217	1.43
	100	1057	1069	954	394	455	414	246	382	381	566	385	943	0.223	1.47
WB_4[a]	0	389.3		437.0	150.7			280.2	224.2		297.0	103.6			2.86
CrB_4[b]	0	554	880	473	254	282	250	65	107	95	265	261			1.02
FeB_4[b]	0	381	710	435	218	114	227	137	143	128	253	177			1.43

[a]Reference[10]

[b]Reference[3]

Table 3. The calculated density ρ (in g/cm^3), the longitudinal, transverse and mean elastic wave velocity (υ_l, υ_t and υ_m in m/s), and the Debye temperature θ_D (in K) of ZrB_4 under pressure.

P	ρ	υ_l	υ_t	υ_m	θ_D
0	5.03	10457	6800	7457	1073
10	5.23	10821	6952	7634	1113
20	5.41	11150	7082	7788	1148
30	5.58	11499	7260	7989	1189
40	5.73	11757	7354	8100	1217
50	5.88	11983	7426	8188	1241
60	6.02	12188	7494	8270	1263
70	6.15	12385	7555	8344	1283
80	6.27	12565	7607	8407	1302
90	6.39	12731	7658	8469	1320
100	6.51	12883	7696	8517	1335

Table 4. The shear anisotropy factors A_1, A_2, A_3 and elastic anisotropy index A^U and the directional bulk modulus B_a, B_b and B_c of ZrB_4 under pressure.

P	A_1	A_2	A_3	A^U	B_a	B_b	B_c
0	1.194	1.173	1.001	0.090	742.4	786.1	655.8
10	1.215	1.249	1.035	0.098	853.7	853.5	775.58
20	1.234	1.280	1.038	0.099	958.3	956.7	885.98
30	1.199	1.260	1.017	0.091	1049.9	1059.1	1002.6
40	1.211	1.288	1.017	0.095	1144.3	1155.6	1112.1
50	1.224	1.319	1.017	0.101	1236.3	1249.5	1222.1
60	1.237	1.348	1.014	0.108	1325.7	1341.3	1322.2
70	1.243	1.369	1.012	0.112	1409.8	1427.7	1438.3
80	1.249	1.392	1.011	0.118	1492.0	1513.1	1553.2
90	1.261	1.425	1.015	0.131	1581.1	1600.7	1646.3
100	1.265	1.443	1.013	0.137	1660.3	1684.5	1755.1

Figure captions

Fig. 1. Pressure dependence of the elastic constants (C_{ij}) of ZrB_4 at 0 K.

Fig. 2. Direction dependence of Young's modulus *E* (a), (d), (g), shear modulus *G* (b), (e), (h) and Poisson's ratio υ (c), (f), (i) under different pressures for ZrB_4, the units are in GPa for *E* and *G*.

Fig. 3. The projections of Young's modulus *E* (a), shear modulus *G* (b) and Poisson's ratio υ (c) in (-110) plane and (001) plane at pressures 0 GPa, 50 GPa and 100 GPa respectively, the units are in GPa for *E* and *G*.

Fig. 4. The calculated normalized volume V/V_0 and bulk modulus of ZrB_4 as a function of pressure at temperatures 0, 200, 400, 600, 800, and 1000 K.

Fig. 5. (a) Temperature dependence of heat capacity at different pressures and (b) Pressure dependence of heat capacity at various temperatures.

Fig. 6. (a) Temperature dependence of thermal expansion coefficient at different pressures. (b) Pressure dependence of the thermal expansion coefficient at various temperatures.

Fig. 7. Debye temperature θ_D (a) and Grüneisen parameter γ (b) for ZrB_4 as a function of pressure at different temperatures.

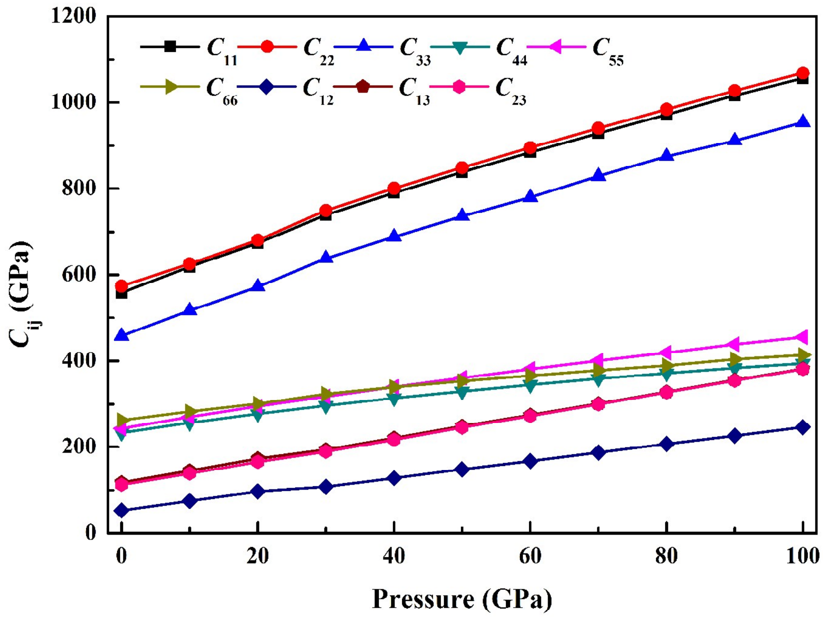

1200
1000
800
600
400
200
0
0
20
40
60
80
100
C_{11}
C_{22}
C_{33}
C_{44}
C_{55}
C_{66}
C_{12}
C_{13}
C_{23}
C_{ij} (GPa)
Pressure (GPa)

Fig. 1

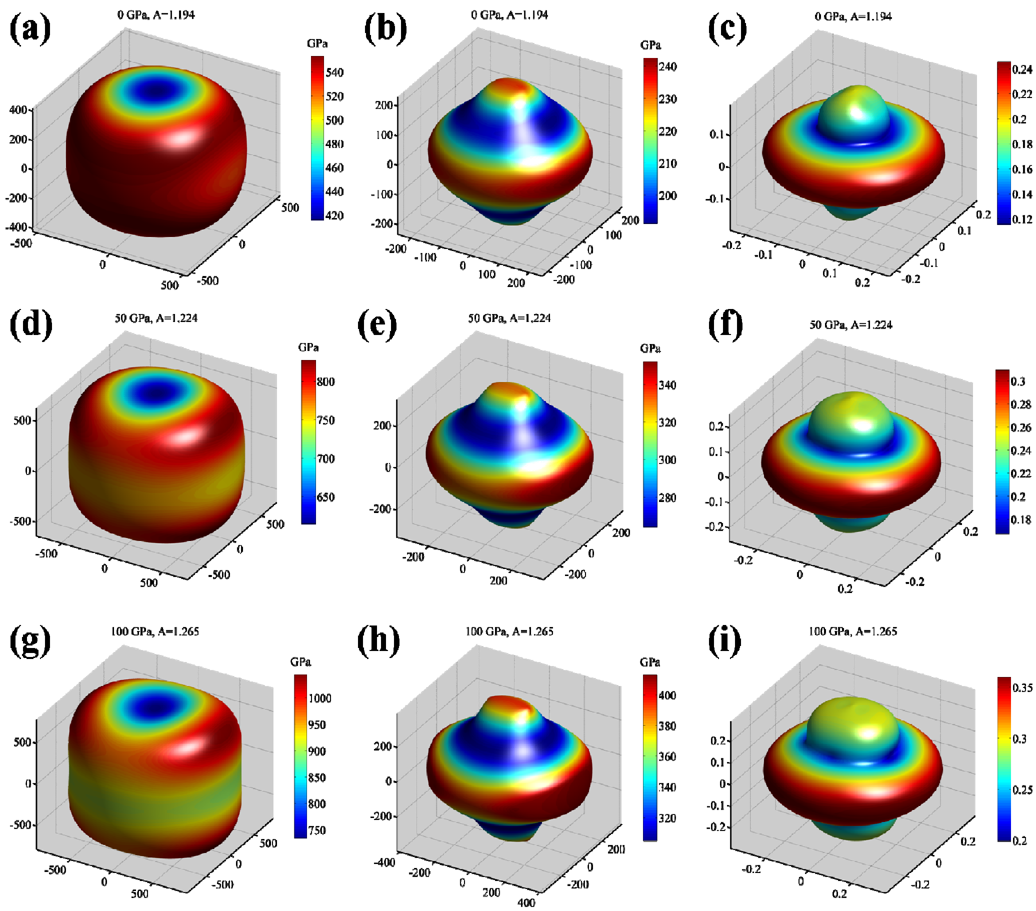
(a)
0 GPa, A=1.194
(b)
0 GPa, A=1.194
(c)
0 GPa, A=1.194
(d)
50 GPa, A=1.224
(e)
50 GPa, A=1.224
(f)
50 GPa, A=1.224
(g)
100 GPa, A=1.265
(h)
100 GPa, A=1.265
(i)
100 GPa, A=1.265
GPa

Fig. 2

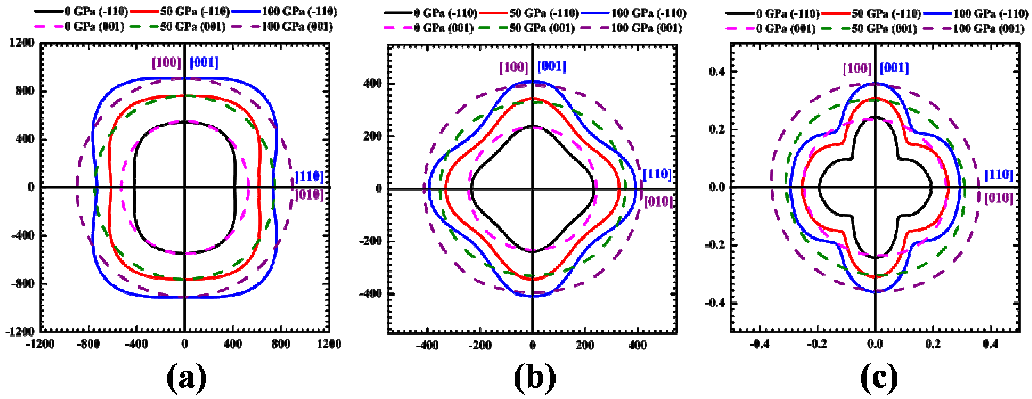
0 GPa (-110)
50 GPa (-110)
100 GPa (-110)
0 GPa (001)
50 GPa (001)
100 GPa (001)
[100]
[001]
[110]
[010]
(a)
(b)
(c)

Fig. 3

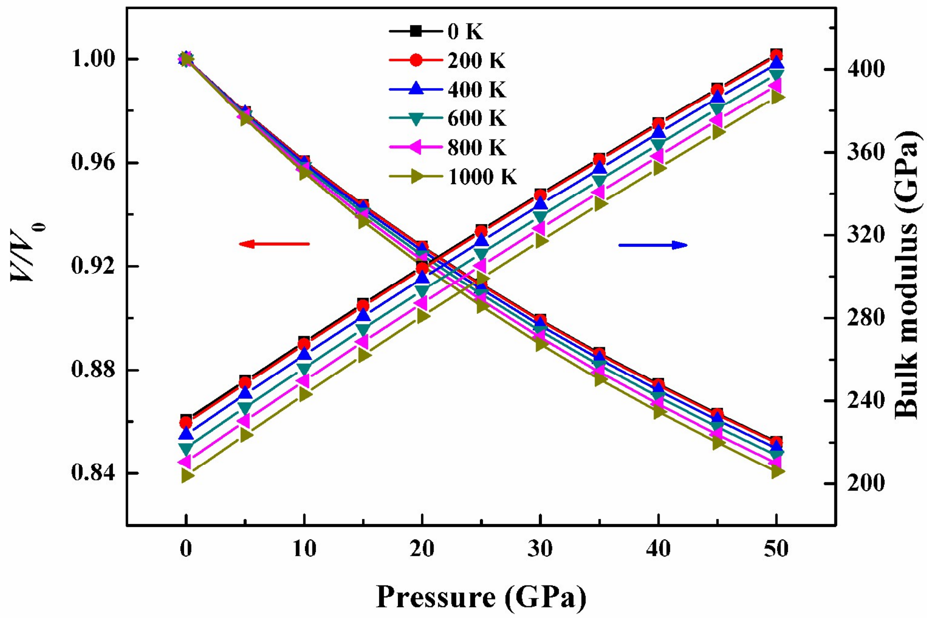

0 K
200 K
400 K
600 K
800 K
1000 K
V/V_0
Bulk modulus (GPa)
Pressure (GPa)
1.00
0.96
0.92
0.88
0.84
400
360
320
280
240
200
0
10
20
30
40
50

Fig. 4

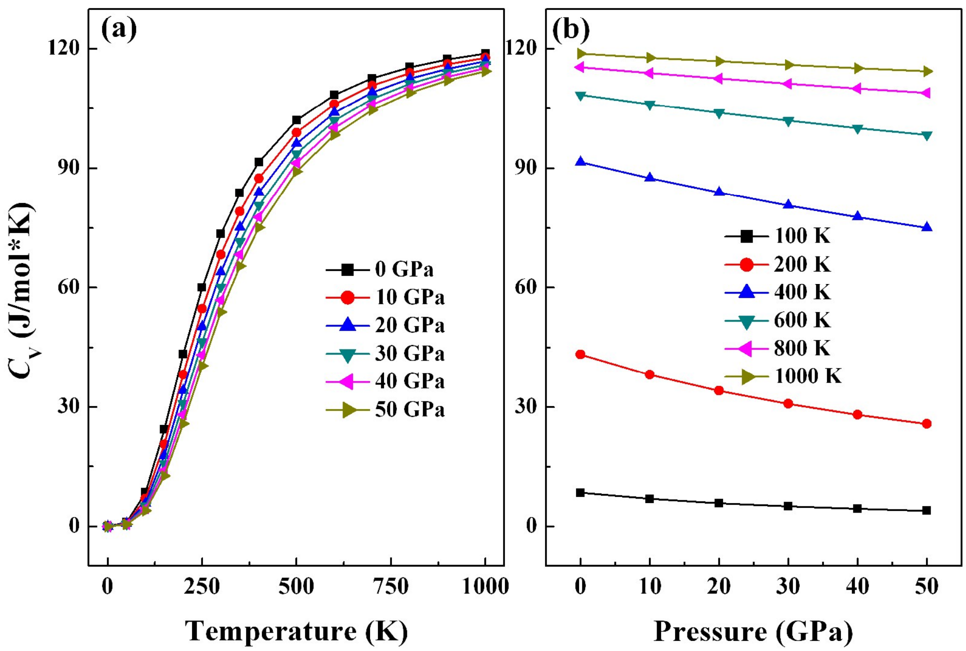
(a)
(b)
C_V (J/mol*K)
0 GPa
10 GPa
20 GPa
30 GPa
40 GPa
50 GPa
100 K
200 K
400 K
600 K
800 K
1000 K
Temperature (K)
Pressure (GPa)

Fig. 5

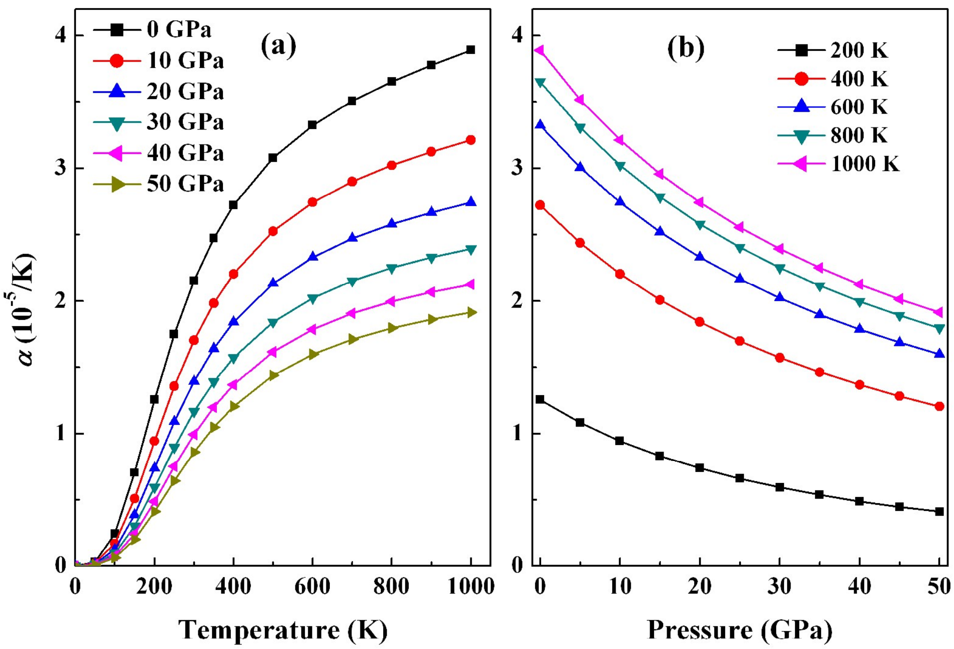

(a)
(b)
0 GPa
10 GPa
20 GPa
30 GPa
40 GPa
50 GPa
200 K
400 K
600 K
800 K
1000 K
α (10⁻⁵/K)
Temperature (K)
Pressure (GPa)

Fig. 6

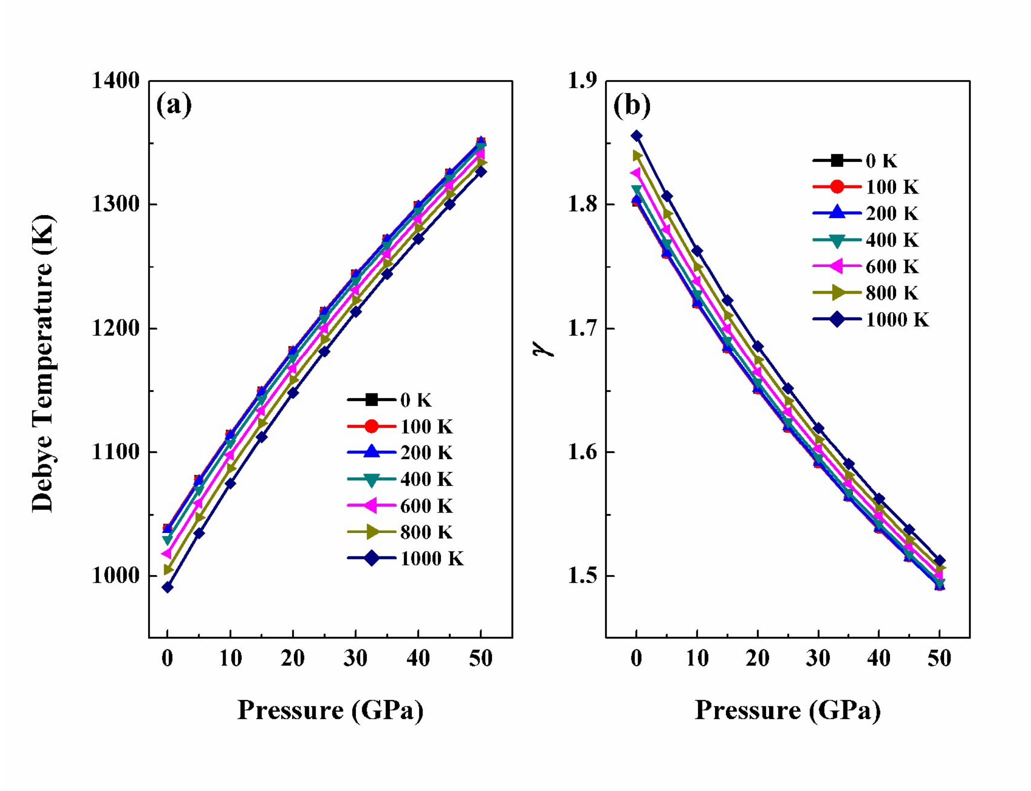
(a)
Debye Temperature (K)
1400
1300
1200
1100
1000
0 10 20 30 40 50
Pressure (GPa)
0 K
100 K
200 K
400 K
600 K
800 K
1000 K
(b)
γ
1.9
1.8
1.7
1.6
1.5
0 10 20 30 40 50
Pressure (GPa)
0 K
100 K
200 K
400 K
600 K
800 K
1000 K

Fig. 7